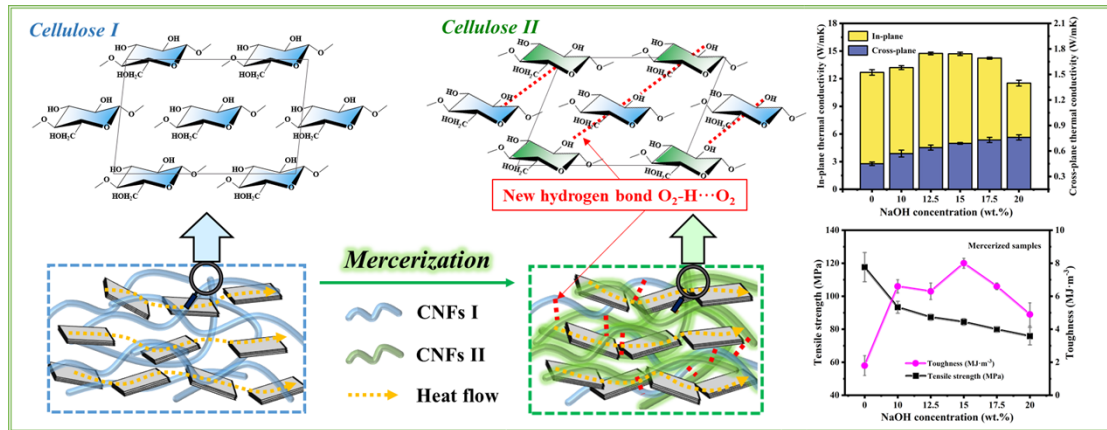


25 Graphical abstract



26
27

28 **Abstract**

29 Generally, the thermal conductivity (*TC*) of composite based on cellulose
30 nanofibrils (CNF) is improved by adding thermal conductive filler, which inevitably
31 leads to the loss of its mechanical properties. In this work, it is the first to
32 simultaneously improve the toughness and *TC* of CNF/boron nitride nanosheets (BNNS)
33 composite from the perspective of thermal conductive filler addition and CNF crystal
34 change. The hydrophilic-modified BNNSs were successfully prepared by xylose-
35 assisted ball-milling prior to adding into CNF. Compared with that of CNF film (1.34
36 W/(m·K)), the in-plane *TC* of CNF/BNNS composite (12.68 W/(m·K)) increased
37 significantly by 846% with loading 30% BNNS. Afterwards, both toughness (8.0
38 MJ·m⁻³, increased ~250 %) and *TC* (14.7 W/(m·K), increased ~16%) of CNF/BNNS
39 composite were further enhanced significantly by mercerization with 12.5% NaOH
40 solution. The simultaneously improvement of toughness and *TC* is unprecedented in
41 related studies, which contributes to the effective preparation of thermal management
42 materials.

43 **Keywords:** Cellulose nanofibrils; Cellulose II; Boron nitride nanosheet;
44 Nanocomposite; Thermal conductivity; Toughness

45 1. Introduction

46 The generation of e-waste from non-degradable materials in advanced electronic
47 devices is putting significant pressure on the environment (Park et al., 2019). The next
48 generation of electronic equipment will require flexibility, miniaturization, integration,
49 and high-power direction development. Thus, there is an urgent need to develop simple,
50 efficient, green, and sustainable materials with flexibility and anisotropic thermal
51 conductivity (TC) in order to achieve proper thermal management (Lao et al., 2018).
52 Naturally abundant cellulose nanofibrils (CNF) are prepared by fibrillation of wood
53 fibers, and these materials have a higher TC (CNF film, in-plane TC , ~ 1.34 W /mK)
54 (Zhang, Tao, Zhang, Liao, & Nie, 2019) than those of most other polymer materials
55 ($0.1\text{--}0.5$ W/(m·K) (C. Chen et al., 2019; M. J. Wang et al., 2018)), which is a strong
56 candidate for heat management materials that are flexible, sustainable, and efficient yet
57 also possess anisotropic thermal conductivity. However, pure CNF films cannot fully
58 satisfy the heat dissipation requirements of electronic devices. Thus, combining the
59 advantages of CNF and high TC fillers is an ideal solution.

60 Hexagonal boron nitride nanosheets (BNNSs) have high TC and electrical
61 insulation, making this material an ideal filler for enhancing the TC of polymer matrix
62 composites (J. Chen, Huang, Sun, & Jiang, 2019). The uniform dispersion of BNNSs
63 in the polymer matrix and the construction of a continuous BNNS thermal conductive
64 network are the key to achieving good mechanical and thermal properties (Shim et al.,
65 2017; Xiao et al., 2015). To achieve these goals, the preparation of hydrophilically-
66 modified BNNSs is an effective way to overcome the interfacial differences between
67 BNNSs and matrix materials to enhance the dispersibility of BNNSs (Z. Liu, Li, & Liu,
68 2020; Yu et al., 2018). However, challenges remain in the mass production of
69 functionalized BNNSs owing to the strong interlayer interaction and chemical inertia
70 of hexagonal boron nitride (h-BN) (W. Lei et al., 2015). Ball-milling with the assistance
71 of a chemical reagent can effectively introduce hydrophilic functional groups onto the
72 edge of BNNSs with a high yield (Lin, Williams, Cao, Elsayed-Ali, & Connell, 2010).

73 However, existing studies' have highlighted a substantial demand for an auxiliary agent
74 (e.g., in the study of urea as auxiliaries, the ratio of auxiliaries to BN was 1:60 (W. Lei
75 et al., 2015) which leads to a lengthy and complex purification process. Therefore, the
76 preparation of functionalized BNNSs in a more efficient, green method is an urgent
77 research topic.

78 So far, there has been a lot of work on the combination of BN with nanocellulose
79 to achieve high *TC* (Hamedi et al., 2014; Z. R. Hu et al., 2018; Nguyen et al., 2018; Wu
80 et al., 2017). Nevertheless, the realization of high *TC* enhancement while remaining the
81 flexibility is still a big challenge because they are incompatible (D. Hu, Huang, Li, &
82 Jiang, 2020; Peng et al., 2017; Yan et al., 2021). Therefore, we examined whether it is
83 possible to enhance the toughness of composites by enhancing the network structure of
84 CNF without losing thermal conductivity of composites due to the reduction of filler.
85 Significantly, the cellulose II crystalline structure has more complex hydrogen bond
86 network and soft crystals than cellulose I (Jaramillo-Quiceno, Velez, Cadena, Restrepo-
87 Osorio, & Santa, 2018; Nakagaito & Yano, 2008; Zhao et al., 2016), which is
88 manifested by the increased thermal stability and toughness of CNF containing
89 cellulose II (CNF II). In order to make use of the advantages of cellulose II and
90 overcome its disadvantage of being difficult to disperse and high-water consumption
91 during mercerization CNFs process (J. Liu & Wang, 2011; Patil et al., 2019), in this
92 study we attempted to mercerize the freshly wet CNF/BNNS composite and control the
93 content of cellulose II in composite film by using different concentrations of NaOH
94 solution.

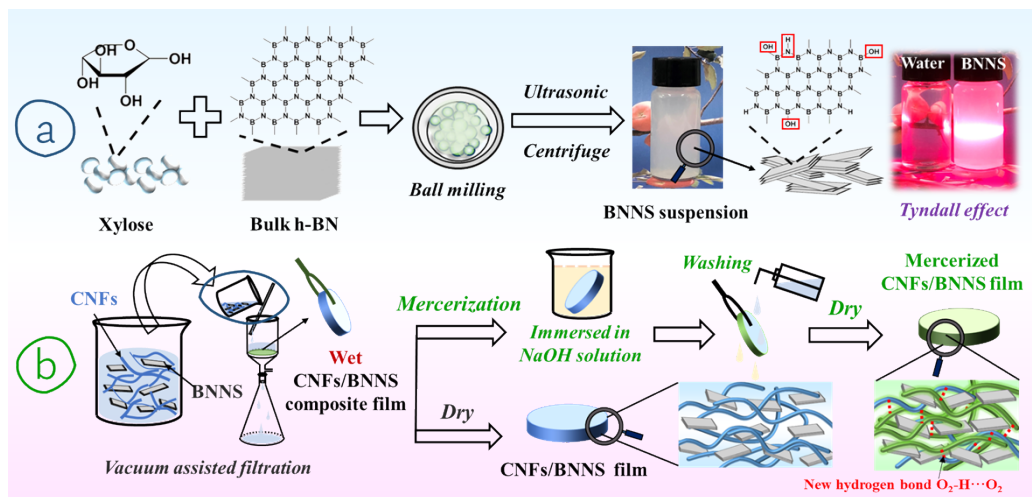
95 In this study, hydrophilically-modified BNNSs were prepared in advance using a
96 xylose-assisted ball milling mechanochemical modification method. The ratio of BNNS
97 to CNF was optimized to obtain the BNNS/CNF composite (0.3-BNNS-CNP) with the
98 best in-plane *TC* (TC_{in}), then the 0.3-BNNS-CNP was mercerized by different
99 concentrations of NaOH to further improve its toughness and *TC*. Finally, the potential
100 of the CNF/BNNS films as a flexible thermal management material was evaluated. This

101 work is the first to take the advantage of cellulose crystal change and thermal
102 conductive filler addition to enhance the structure of CNF-based composite materials,
103 which will promote the effective preparation of thermal management materials.

104 2. Experimental

105 Hexagonal boron nitride (h-BN, particle size: 30 μm , 99.5%) powder was
106 purchased from ENO High-Tech Material Development Co., Ltd. (China). D-xylose
107 (analytical reagent grade) and sodium hydroxide (reagent grade, 97%) were obtained
108 from Sigma-Aldrich (USA). Bleached kraft softwood pulp board was obtained from
109 Yun-Jing Forestry & Pulp Mill Co., Ltd., (China). The method for preparing CNF was
110 similar to our previous work, with a grinding time of 2 h and samples homogenized 10
111 times (Xu et al., 2021), and the diameter of the CNF was 56 nm (Fig. S1).

112 Fig. 1 shows the preparation process of BNNSs (Fig. 1a), CNF/BNNS composite
113 films and the mercerization process (Fig. 1b). The materials, details procedures of
114 preparation and characterization were listed in the Supplementary.



115

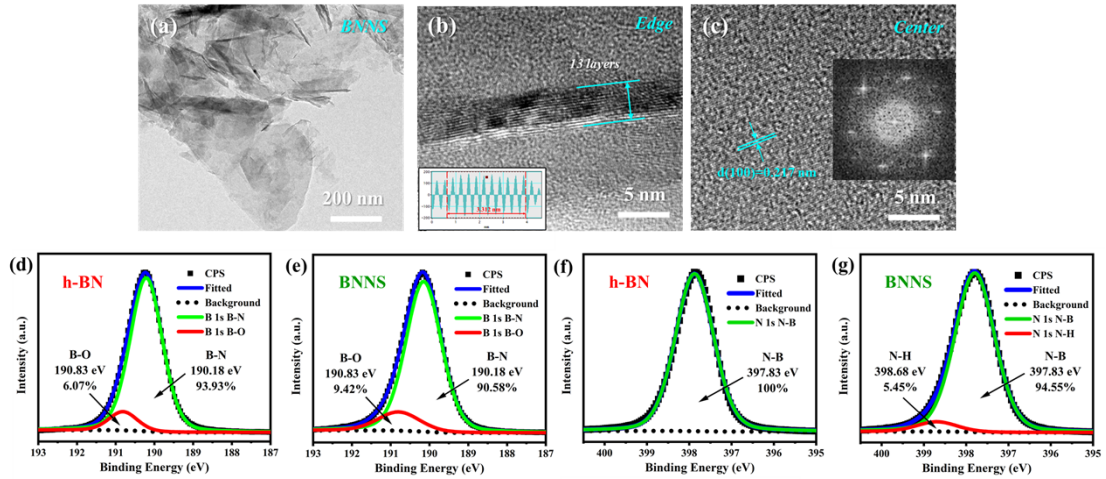
116 Fig.1. Preparation process of BNNSs and mercerization of CNF/BNNS composite film

117 3. Results and discussion

118 3.1 Characterization analysis of BNNSs

119 Hydrophilic BNNSs were prepared successfully by xylose assisted ball milling to

120 improve the interface between CNF and BNNSs. As shown in Fig. 2a and 2b, the
121 BNNSs showed a thin sheet with a height of several nanometers and a high aspect ratio.
122 According to statistical analysis by AFM (Fig. S2) and TEM (Fig. S3), the average
123 height and lateral size of BNNSs prepared were ~4.5 nm and ~254 nm, respectively.
124 The well-ordered lattice structure in the in-plane central region of BNNSs could be
125 observed in the HR-TEM image (Fig. 2c), which is the key for BNNS to achieve high
126 *TC* (Guerra, Wan, & McNally, 2019). Besides, the particular hexagonal symmetry of
127 BNNSs was also shown in the fast Fourier transform (FFT) image (illustration in Fig.
128 2c) that indicated exfoliated BNNSs had a hexagonal crystal structure. As shown in Fig.
129 2d and 2e, compared with the B-O peak area of h-BN (6.07%), the B-O peak area of
130 BNNSs increased to 9.42%, revealing that many B-O bonds were introduced into
131 BNNSs after xylose-assisted ball milling. As shown in Fig. 2f and 2g, only N-B (397.83
132 eV) existed in the N 1s spectrum of h-BN (Fig. 3c), whereas both N-B (397.83, 94.55%)
133 and N-H peaks (398.68 eV, 5.45%) were present in the N 1s spectrum of BNNSs (Fig.
134 3d), indicating that there were N atoms bonded to H atoms in BNNSs. The additional
135 evidence of BN modification will be analyzed in detail in Supplementary (Fig. S4, S5,
136 S6, and Table S1). Briefly, xylose-assisted ball-milling method is highly efficient in
137 preparing functionalized BNNS with hydrophilic functional groups (hydroxyl and
138 amino groups), and hundreds of hours could be saved compared to the ultrasound
139 approach (Z. D. Wang et al., 2020; Z. G. Wang et al., 2021).



140

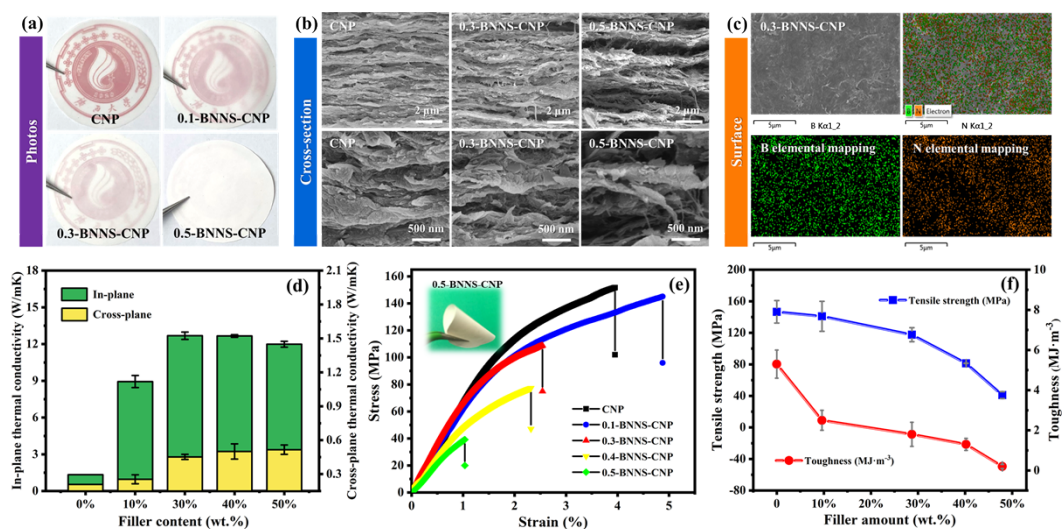
141 Fig.2. Morphology and chemical group analysis of BN: HR-TEM image of (a) BNNSs, (b)
 142 center (inset with fast Fourier transform (FFT) image) and (c) edge (inserted with selected-
 143 area electron diffraction (SAED) mode images), and XPS analysis of B 1s (d, e) and N 1s (f,
 144 g).

145 3.2 Property characterizations of CNF/BNNS composite films

146 The effect of the BNNS content on the morphology, TC_{in} and TC_{cross} , and
 147 mechanical properties of the CNF/BNNS composite films are shown in Fig. 3. The
 148 initial thermal decomposition temperature of all the CNF/BNNS films was more than
 149 305 °C according to the TGA which ensures its safety in use. The photos (Fig. 3a)
 150 showed that the color of the CNF/BNNS films tended to be opaque white with an
 151 increase in the BNNS amount. The fracture surfaces (Fig. 3b) of all CNF/BNNS films
 152 had a typical layered structure. The fillers were arranged in an orderly manner along
 153 with the CNF layers. This structure was beneficial for the heat dispersion along the
 154 plane (An et al., 2021). And BNNSs were uniformly dispersed in the composites
 155 without serious agglomeration from the B and N elemental mapping (Fig. 3c), ensuring
 156 the uniformity of the composite material. However, the fillers contacted each other at a
 157 high amount of BNNSs (approximately 50 wt.%), possibly causing phonon scattering
 158 in the main direction of heat transfer and resulting in decreased TC of the material.
 159 Moreover, the failure of the continuous layered network structure of CNF caused by
 160 excessive addition prevented the composites from achieving better mechanical

161 properties. The 0.3-BNNS-CNP had a uniform mixture of CNF and BNNSs and
162 maintained the layered structure characteristic of CNF. As shown in Fig. 3d, the 0.3-
163 BNNS-CNP had the best TC_{in} , 12.68 W/(m·K), of all the samples, and this value was
164 more than nine times that of the CNF film. The anisotropic TC materials, high TC_{in}
165 and low cross-plane TC (TC_{cross}) can realize the efficient transfer of heat along the in-
166 plane direction while protecting the devices on both sides of the cooling film from
167 excessive heat (C. X. Lei et al., 2019). The anisotropy of the TC of the composites was
168 calculated (Table S3). The 0.3-BNNS-CNP showed high anisotropy thermal
169 conductivity (a TC_{in}/TC_{cross} ratio of 28) that was comparable to that of an oriented
170 BNNS (33 wt.%) and polyvinylidene fluoride (PVDF) composite film (a TC_{in}/TC_{cross}
171 ratio of 21) (J. Chen et al., 2019).

172 The stress-strain curves and the tensile strength and toughness as a function of filler
173 content are shown in Fig. 3e and 3f, respectively. Specific data for mechanical
174 properties are shown in Table S4. The tensile strengths and toughness of 0.1-BNNS-
175 CNP, 0.3-BNNS-CNP, 0.4-BNNS-CNP, and 0.5-BNNS-CNP were 140.96 MPa and
176 $2.5 \text{ MJ}\cdot\text{m}^{-3}$, 117.63 MPa and $1.8 \text{ MJ}\cdot\text{m}^{-3}$, 81.31 MPa and $1.3 \text{ MJ}\cdot\text{m}^{-3}$, and 41.05 MPa
177 and $0.2 \text{ MJ}\cdot\text{m}^{-3}$, respectively. The mechanical strength of the CNF-based films was
178 dominated by the hydrogen bonding forces, van der Waals forces, and interwinding
179 forces between the CNFs (Niinivaara & Cranston, 2020). The tensile strength of
180 composites with a low loading of BNNSs ($\sim 10 \text{ wt.}\%$) decreased slightly because of the
181 transfer of stress from CNFs to BNNSs. With an increase in BNNS loading (over 30
182 wt.%), the tensile strength and elongation at the break of composites decreased sharply
183 due to the weakening of the interface strength between CNF and BNNSs. In brief, 0.3-
184 BNNS-CNP maintained a good balance between the different properties under
185 investigation, with a tensile strength of 117.63 MPa, an elongation at break of 2.88 %,
186 an TC_{in} of 12.68 W/(m·K), which is an increase of 846% compared with CNF film
187 ($1.34 \text{ W}/(\text{m}\cdot\text{K})$).



188

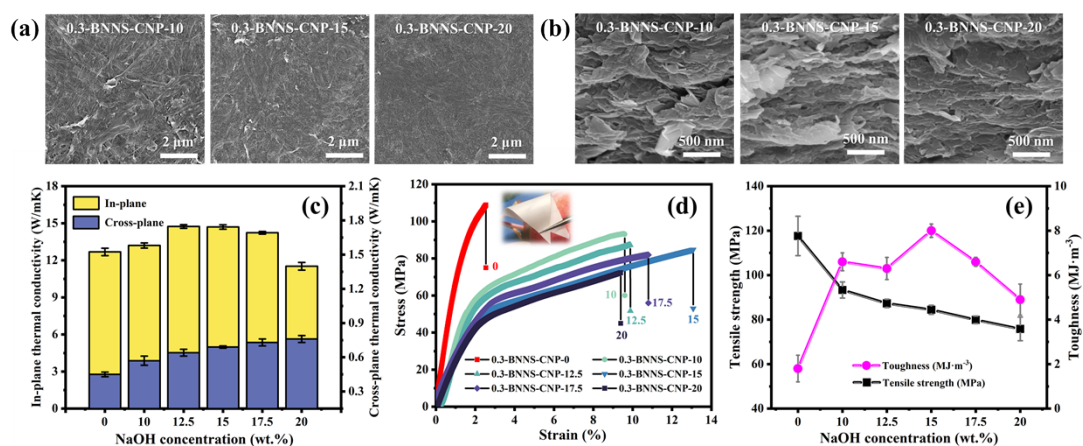
189 Fig.3. Physical properties of films: (a) Photographs, (b) cross-section FE-SEM images, (c)
 190 surface FE-SEM image of 0.3-BNNS-CNP and its B and N elemental mapping, (d) TC_{in} and
 191 TC_{cross} , (e) stress-strain curves (inserted with the flexibility of 0.5-BNNS-CNP), and (f)
 192 tensile strength and toughness.

193 3.3 Improved performance of CNF/BNNS films by mercerization

194 The comprehensive properties of the CNF/BNNS composites were further
 195 improved from the perspective of crystalline structure of cellulose by mercerizing 0.3-
 196 BNNS-CNP. First, the surface and cross-sectional morphologies of the mercerized
 197 samples were analyzed (Fig. S9). With an increase in the degree of mercerization, the
 198 surfaces of the composites became smoother (Fig. 4a), and the cross-sectional structure
 199 was more compact (Fig. 4b). Moreover, mercerization did not change the layered
 200 structure of the composite material (Fig. 4b).

201 Then the influence of mercerization on the TC_{in} and TC_{cross} of composites are
 202 analyzed. As shown in Fig. 4c and Table S5, the TC_{in} of the sample mercerized at a
 203 concentration of 12.5 wt.% alkali solution was 14.74 W/(m·K), an increase of ~16%
 204 compared to the un-mercerized sample (12.68 W/(m·K)) and the best of the mercerized
 205 ones. The TC_{cross} of the samples increased slightly from 0.45 W/(m·K) to 0.76 W/(m·K).
 206 The above phenomena indicate that a moderate mercerization treatment was beneficial
 207 to improving the TC of the CNF/BNNS composites. In addition, the specific values of

208 tensile strength, elongation at break, and toughness of the mercerized samples are
 209 summarized in Table S6. As shown in Fig. 4d and Fig. 4e, although the tensile strength
 210 decreased from 117.63 MPa to 87.31 MPa after moderate mercerization, the toughness
 211 of 0.3-BNNS-CNP increased significantly from 1.8 MJ·m⁻³ to 8.0 MJ·m⁻³. In
 212 conclusion, mercerization significantly improved the toughness and *TC* of the
 213 CNF/BNNS composite.



214
 215 Fig.4. Analysis of mercerized films: FE-SEM images of (a) the surface and (b) fracture
 216 surface, (c) TC_{in} and TC_{cross} , (d) stress-strain curves (inserted with the flexibility of 0.3-
 217 BNNS-CNP-12.5), and (e) tensile strength and toughness.

218 Herein, we discuss the mercerization mechanism for enhancing the *TC* and
 219 toughness of CNF/BNNS composite films. The *TC* of composites is commonly
 220 determined by the matrix material and thermal filler (L. Chen et al., 2016). For thermal
 221 filler, since the diffraction peak of (100) crystal plane (at 41.5°) of BNNS is obvious
 222 based on the XRD test (Fig. S5a), the BNNS powder is disordered. However, as shown
 223 in Fig. 5a, the XRD peaks at 41.5° of BNNSs in mercerized samples were disappear,
 224 which suggested that BNNS filler was arranged regularly along the in-plane direction
 225 in the films rather than a disordered arrangement (Wu et al., 2017). Thus, the regular
 226 arrangement of BNNS in the in-plane direction of CNF/BNNS composite can enhance
 227 the TC_{in} of composite. For the matrix material, CNF dissipates heat through the
 228 vibration of cellulose crystalline region (Uetani, Okada, & Oyama, 2015). Some studies

229 also think that the destruction of crystallization region of cellulose can result in a
 230 decrease in the TC of CNF (Lee, Sundaram, Zhu, Zhao, & Mani, 2018). As shown in
 231 Fig. 5b, cellulose crystallinity in the mercerized CNF/BNNS composites decreased
 232 from 62.81% to 43.42% when the amount of lye increased from 0 wt.% to 20 wt.%.
 233 The TC_{in} of 0.3-BNNS-CNP-12.5 mercerized by 12.5 wt.% alkali solution has the best
 234 TC_{in} value, 14.74 W/(m·K), of all the samples (Fig. 5c). Therefore, combined with the
 235 analysis of XRD and TC results, we can reasonably think that the TC_{in} improvement of
 236 properly mercerized films can be attributed to the internal morphology change of
 237 composite films caused by mercerization, that is, due to a dense internal structure of the
 238 composite, an improved in-plane orientation of BNNSs in the composites, and an
 239 enhanced CNF network structure.

240 The denser internal structure of the material can be reflected in density changes.
 241 Thus, we calculated the theoretical density and void fraction of the composites using
 242 the following formula (1,2):

$$243 \quad \rho_1 = \frac{1}{\frac{V_{\text{BNNS}}}{\rho_{\text{BNNS}}} + \frac{V_{\text{CNFs}}}{\rho_{\text{cellulose}}}} \quad (1),$$

$$244 \quad \text{Void fraction} = \frac{\rho_1 - \rho_2}{\rho_1} \quad (2),$$

245 where ρ_{BNNS} and $\rho_{\text{cellulose}}$ are the densities of BNNSs (2.29 g/m³) and cellulose (1.5
 246 g/cm³), respectively (X. Wang et al., 2020; Xu et al., 2021); w_{BNNS} and w_{CNF} are the
 247 loading amounts of BNNSs and CNF, respectively (the actual amount of BNNSs in the
 248 composite was corrected by the TGA analysis of the residual mass at 800 °C, as shown
 249 in Table S2 and Fig. S7); and ρ_2 is the experimental density of the composites (Fig. 5c
 250 and Fig. 5d). As shown in Fig. 5c, the void fraction decreased from ~0.17 to ~0.06 as
 251 the amount of BNNSs added increased from 0 wt.% to 50 wt.%, indicating that
 252 hydroxylated BNNSs effectively filled the voids of the fiber network structure in the
 253 composites. After mercerization, the experimental density of films increased from
 254 approximately 1.5 g/cm³ to 1.6 g/cm³ (Table S5), whereas the void fraction decreased
 255 from ~0.09 to ~0.01 (Fig. 5d). These results indicated that the densification of the

256 CNF/BNNS composite film was significantly enhanced by adding fillers to BNNSs and
257 mercerization.

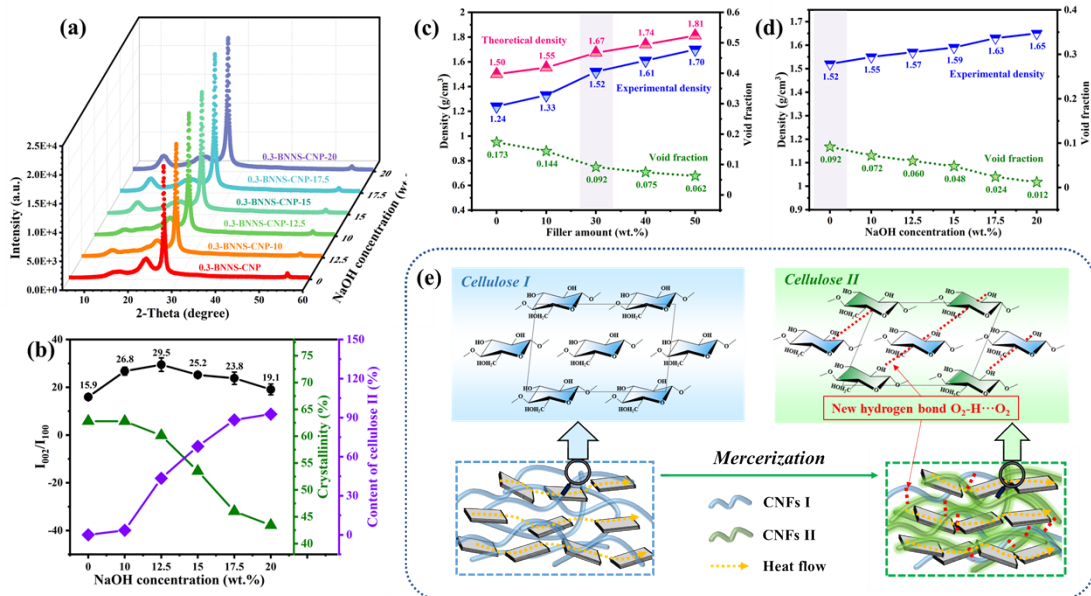
258 The ratio of the peak intensities ($I_{(002)}/I_{(100)}$) at 26.5° and 41.5° of the samples were
259 calculated to analyze the in-plane orientation degree of BNNSs in the mercerized films,
260 as summarized in Fig. 5b (Wu et al., 2017). As shown in Fig. 5b, the $I_{(002)}/I_{(100)}$ ratio
261 increased after moderate mercerization, but further increases in mercerization led to a
262 decrease in this value, which indicated that the in-plane orientation of BNNSs in the
263 composites was improved by moderate mercerization. That is, the 0.3-BNNS-CNP-
264 12.5 was treated with 12.5 wt.% NaOH solution had an TC_{in} of 14.74 W/(m·K) that
265 represented an approximately 16% increase compared with that of the 0.3-BNNS-CNP.

266 The reasons for the low TC_{cross} of the composites could be mainly divided into two
267 aspects. One is the increase of film thickness after mercerization (from 29.5 μm to 39.8
268 μm by 15 wt.% lye mercerized). This increases the distance required for heat transfer.
269 Second, BNNSs typically has a two-dimensional sheet structure with highly TC_{in} and
270 poorly TC_{cross} themselves, and most of the BNNS are arranged along the plane inside
271 of the composite (Wu et al., 2018).

272 Cellulose II crystals are well known to have higher toughness but lower strength
273 than cellulose I (Sharma, Nair, Zhang, Ragauskas, & Deng, 2015), that is attributed to
274 the softening of cellulose crystals by mercerization and beneficial to the enhancement
275 of fiber toughness (H. Y. Wang, Li, Yano, & Abe, 2014). After mercerization, all 0.3-
276 BNNS-CNP samples with different degrees of mercerization exhibit the diffraction
277 peaks of cellulose II crystalline structure at $2\theta = 12.0^\circ$ and 21.6° in Fig. S10, indicating
278 that the mercerization treatment transformed the crystalline structure of cellulose in the
279 composites from I to II (Gupta, Uniyal, & Naithani, 2013). Jade software (version 6.0)
280 was used to calculate the content of cellulose II in composite, and the results (Fig. 5b
281 and Table S7) show that the content of cellulose II increased continuously with
282 increasing alkali concentration, reaching approximately 93% after treated with 20 wt.%
283 lye. Above all, the study of O'Sullivan et al has proved that the presence of cellulose II

284 in cellulose can declare the production of new hydrogen bonds ($O_2-H\dots O_2$ and $O_6-H\dots$
285 O_2) (O'Sullivan, 1997). Thus, we think that the increase of cellulose II content in the
286 composites also can demonstrate the formation of new hydrogen-bonding.

287 Then, the enhancement principle of mercerization on mechanical properties of the
288 composites are analyzed. The CNFs have firstly formed a network structure due to
289 hydrogen bonds and van der Waals force during filtration (Niinivaara & Cranston,
290 2020). After mercerizing the wet CNF/BNNS film, the swelling agents (NaOH) are
291 removed by washing method, the cellulose crystals are rearranged and converted from
292 cellulose I to cellulose II, and the structure of CNF/BNNS film is enhanced by new
293 hydrogen bonds ($O_2-H\dots O_2$ and $O_6-H\dots O_2$) formed by cellulose II crystalline
294 transformation (O'Sullivan, 1997). Then, the adhesion among fibers can be improved.
295 Therefore, a compact CNFs/BNNS composite film mercerized by NaOH solution can
296 been obtained (Kolpak & Blackwell, 1976; Nomura, Kugo, & Erata, 2020). These
297 changes in the CNF reduced the interspace between BNNSs. The mercerized film
298 maintained the original layered structure that promoted the formation of a continuous
299 thermal conduction network between BNNSs. To sum up, the enhancement of the
300 structure of the CNF/BNNS composite films by mercerization can be summarized as
301 follows: 1) CNF swelled in lye and then dehydrated and shrunken after washing. The
302 cellulose chains between fibers diffused, improving the compactness of the composite
303 films. 2) The moderate transformation of the crystalline structure from cellulose I→II
304 in the CNF/BNNS composite films increased the number of hydrogen bonds and
305 enhanced the complexity of the hydrogen bond network structure in the CNF/BNNS
306 composite films.



307

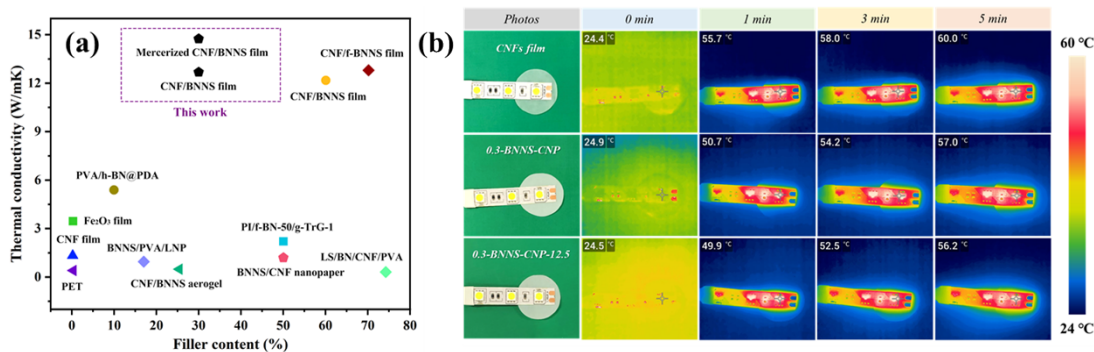
308 Fig.5. Effect of mercerization on the CNF/BNNS films: (a) the XRD characteristic peak region
 309 of mercerized films; (b) effects of mercerization on the $I_{(002)}/I_{(100)}$ ratio, cellulose crystallinity,
 310 and content of cellulose II; (c) curves of theoretical density, experimental density, and void
 311 fraction of films with different filler amounts; (d) curves of theoretical density, experimental
 312 density, and void fraction with different mercerization degrees; and (e) schematic diagram of
 313 how mercerization enhanced the hydrogen bond structure of the film.

314 3.4 Comparison and application

315 As shown in Fig. 6a and Table S8, compared to the TC_{in} of the previous reports (Z.
 316 R. Hu et al., 2018; Y. Liu et al., 2020; Shen, Guo, Wang, Zhao, & Xu, 2015; Tsai,
 317 Tseng, Chiang, & Li, 2014; X. Wang et al., 2020; X. Wang et al., 2022; X. Wang et al.,
 318 2019; Wu et al., 2017; Wu et al., 2018), we found that most of the studies aimed to
 319 improve the interface between CNFs and BNNSs by modifying BNNSs in different
 320 ways to realize the construction of a heat transfer network. In this study, the CNF
 321 composite film's thermal conductivity was firstly improved by introducing a
 322 hydrophilic modification of BNNSs at a low loading amount (~30 wt.%). Then, unlike
 323 other studies, in order to improve the toughness loss of composite films due to the
 324 addition of inorganic particles, the wet films were mercerized, and the toughness of the
 325 CNF/BNNS composite films was further improved (increased by ~250%) and
 326 simultaneously the high thermal conductivity was achieved (enhanced by

327 approximately 16%). This ensures the application of the nanocomposite as a flexible
 328 heat management material.

329 To visually observe the heat dissipation capacity, the film samples were attached
 330 to the back of a LED chip, and an infrared camera was used to photograph the samples
 331 and record the temperature change of the LED every 30 s. The temperatures of a CNF
 332 film, 0.3-BNNS-CNP, and 0.3-BNNS-CNP-12.5 were measured and recorded as T_1 ,
 333 T_2 , and T_3 , respectively. As shown in Fig. 6b, the temperatures of the LEDs on the three
 334 samples were approximately the same at the start. As time passed, the temperatures of
 335 T_2 and T_3 at the same time were significantly lower than T_1 , and the temperature
 336 difference between the three samples increased gradually with time. For example, when
 337 the LED chip was operated for 1 min, T_1 , T_2 , and T_3 were respectively 55.7 °C, 50.7
 338 °C, and 49.9 °C, with a maximum difference of 5.8 °C. When the LED chip was
 339 operated for 5 min, T_1 , T_2 , and T_3 were respectively 60.0 °C, 57.0 °C, and 56.2 °C. The
 340 results showed that the CNF/BNNS composite film exhibited the ability for timely heat
 341 dissipation, and the heat generated by the LED chip was released promptly. The timely
 342 heat dissipation capacity of CNF film was significantly enhanced by introducing
 343 BNNSs and the mercerization of the wet film, which further enhanced the application
 344 of CNF. Therefore, the 0.3-BNNS-CNP-12.5 has both flexibility and promising heat
 345 dissipation capacity, which has great potential to be used as a heat dissipation material
 346 for electronic devices.



347
 348 Fig.6. (a) Comparison of the thermal conductivities of composites based on boron nitride,
 349 conventional metals and plastics, and (b) Optical and thermal images of the light-emitting

350 diode (LED) chips attached to the CNF film, 0.3-BNNS-CNP, and 0.3-BNNS-CNP-12.5.

351 **4. Conclusion**

352 In this work, hydrophilic-modified BNNSs were successfully obtained by the
353 mechanochemical process of ball milling assisted with xylose, and hydroxylated
354 BNNSs improved the compatibility of CNF and BNNSs. The 0.3-BNNS-CNP
355 maintained good comprehensive properties, with a tensile strength of 117.63 MPa,
356 elongation at break of 2.88%, a TC_{in} of 12.68 W/(m·K), which is an increase of 846%
357 compared with CNF film (TC_{in} , 1.34 W/(m·K)). Furthermore, unlike other studies, in
358 order to improve the toughness loss of composite films due to the addition of inorganic
359 particles, the wet CNF composite films were mercerized, and the toughness of the
360 CNF/BNNS composite films was further improved (increased by ~250%) and
361 simultaneously the high thermal conductivity was achieved (enhanced by
362 approximately 16%) by 12.5 wt.% lye mercerization. This mercerized 0.3-BNNS-CNP-
363 12.5 film shows a good combination of thermal conductivity, thermal stability,
364 flexibility, and mechanical strength. Therefore, this mercerized BNNS-CNP film
365 presents great potential applications in flexible electronic equipment.

366 **Acknowledgment**

367 The project was sponsored by the National Key Research and Development
368 Program of China (grant no. 2021YFE0114400), Natural Science Foundation of
369 Guangxi Province, China (grant no. 2021GXNSFDA196006), and the Foundation of
370 Guangxi Key Laboratory of Clean Pulp & Papermaking and Pollution Control, College
371 of Light Industry and Food Engineering, Guangxi University (grant nos. 2021KF20,
372 2021KF02, and 2021KF32). AJR efforts were supported by the University of
373 Tennessee, Knoxville.

374 **Competing Interest Statement:**

375 The authors declare no competing interest.

376 **Credit author statement:**

377 **Ying Xu**, Conceptualization, Investigation, Formal analysis, Data curation,
378 Visualization, Writing- original draft preparation. **Xinrui Chen and Caixia Zhang**,
379 Investigation, Formal analysis, Data curation, Writing. **Arthur J. Ragauskas**,
380 Resources, Project administration. **Jialong Wen**, Validation, Writing- Review &
381 Editing. **Peitao Zhang, Ting Xu and Chuanling Si**, Formal analysis, Supervision.
382 **Xueping Song**, Conceptualization, Project administration, Methodology, Resources,
383 Writing- Review & Editing, Funding acquisition.

384 **References**

- 385 An, L., Gu, R., Zhong, B., Wang, J., Zhang, J., & Yu, Y. (2021). Quasi-isotropically
386 thermal conductive, highly transparent, insulating and super-flexible polymer
387 films achieved by cross linked 2D hexagonal boron nitride nanosheets. *Small*,
388 17(46), 2101409.
- 389 Chen, C., Xue, Y., Li, Z., Wen, Y. F., Li, X. W., Wu, F., . . . Xie, X. L. (2019).
390 Construction of 3D boron nitride nanosheets/silver networks in epoxy-based
391 composites with high thermal conductivity via in-situ sintering of silver
392 nanoparticles. *Chemical Engineering Journal*, 369, 1150-1160.
- 393 Chen, J., Huang, X., Sun, B., & Jiang, P. (2019). Highly thermally conductive yet
394 electrically insulating polymer/boron nitride nanosheets nanocomposite films
395 for improved thermal management capability. *ACS Nano*, 13(1), 337-345.
- 396 Chen, L., Sun, Y. Y., Xu, H. F., He, S. J., Wei, G. S., Du, X. Z., & Lin, J. (2016).
397 Analytic modeling for the anisotropic thermal conductivity of polymer
398 composites containing aligned hexagonal boron nitride. *Composites Science and*
399 *Technology*, 122, 42-49.
- 400 Guerra, V., Wan, C. Y., & McNally, T. (2019). Thermal conductivity of 2D nano-
401 structured boron nitride (BN) and its composites with polymers. *Progress in*
402 *Materials Science*, 100, 170-186.

403 Gupta, P. K., Uniyal, V., & Naithani, S. (2013). Polymorphic transformation of
404 cellulose I to cellulose II by alkali pretreatment and urea as an additive.
405 *Carbohydrate Polymers*, 94(2), 843-849.

406 Hamed, M. M., Hajian, A., Fall, A. B., Hakansson, K., Salajkova, M., Lundell, F., . . .
407 Berglund, L. A. (2014). Highly conducting, strong nanocomposites based on
408 nanocellulose-assisted aqueous dispersions of single-wall carbon nanotubes.
409 *ACS Nano*, 8(3), 2467-2476.

410 Hu, D., Huang, X., Li, S., & Jiang, P. (2020). Flexible and durable cellulose/MXene
411 nanocomposite paper for efficient electromagnetic interference shielding.
412 *Composites Science and Technology*, 188, 107995.

413 Hu, Z. R., Wang, S., Chen, G. K., Zhang, Q., Wu, K., Shi, J., . . . Lu, M. G. (2018). An
414 aqueous-only, green route to exfoliate boron nitride for preparation of high
415 thermal conductive boron nitride nanosheet/cellulose nanofiber flexible film.
416 *Composites Science and Technology*, 168, 287-295.

417 Jaramillo-Quiceno, N., Velez, J. M., Cadena, E. M., Restrepo-Osorio, A., & Santa, J.
418 F. (2018). Improvement of mechanical properties of pineapple leaf fibers by
419 mercerization process. *Fibers Polymers*, 19(12), 2604-2611.

420 Kolpak, F. J., & Blackwell, J. (1976). Determination of the structure of cellulose II.
421 *Macromolecules*, 9(2), 273-278.

422 Lao, J. P., Xie, H. A., Shi, Z. Q., Li, G., Li, B., Hu, G. H., . . . Xiong, C. X. (2018).
423 Flexible regenerated cellulose/boron nitride nanosheet high-temperature
424 dielectric nanocomposite films with high energy density and breakdown
425 strength. *ACS Sustainable Chemistry & Engineering*, 6(5), 7151-7158.

426 Lee, H., Sundaram, J., Zhu, L., Zhao, Y., & Mani, S. (2018). Improved thermal stability
427 of cellulose nanofibrils using low-concentration alkaline pretreatment.
428 *Carbohydrate Polymers*, 181, 506-513.

429 Lei, C. X., Wu, K., Wu, L. Y., Liu, W. J., Du, R. N., Chen, F., & Fu, Q. (2019). Phase
430 change material with anisotropically high thermal conductivity and excellent

431 shape stability due to its robust cellulose/BNNSs skeleton. *Journal of Materials*
432 *Chemistry A*, 7(33), 19364-19373.

433 Lei, W., Mochalin, V. N., Liu, D., Qin, S., Gogotsi, Y., & Chen, Y. (2015). Boron
434 nitride colloidal solutions, ultralight aerogels and freestanding membranes
435 through one-step exfoliation and functionalization. *Nature Communications*, 6,
436 8849.

437 Lin, Y., Williams, T. V., Cao, W., Elsayed-Ali, H. E., & Connell, J. W. (2010). Defect
438 functionalization of hexagonal boron nitride nanosheets. *Journal of Physical*
439 *Chemistry C*, 114(41), 17434-17439.

440 Liu, J., & Wang, F. M. (2011). Influence of mercerization on micro-structure and
441 properties of kapok blended yarns with different blending ratios. *Journal of*
442 *engineered fibers and fabrics*, 6(3), 63-68.

443 Liu, Y., Zhang, Y., Liao, T., Gao, L., Wang, M., Xu, X., . . . Liu, H. (2020). Boron
444 nitride–nanosheet enhanced cellulose nanofiber aerogel with excellent thermal
445 management properties. *Carbohydrate Polymers*, 241, 116425.

446 Liu, Z., Li, J., & Liu, X. (2020). Novel functionalized BN nanosheets/epoxy composites
447 with advanced thermal conductivity and mechanical properties. *ACS Applied*
448 *Materials & Interfaces*, 12(5), 6503-6515.

449 Nakagaito, A. N., & Yano, H. (2008). Toughness enhancement of cellulose
450 nanocomposites by alkali treatment of the reinforcing cellulose nanofibers.
451 *Cellulose*, 15(2), 323-331.

452 Nguyen, H. L., Hanif, Z., Park, S. A., Choi, B. G., Tran, T. H., Hwang, D. S., . . . Oh,
453 D. X. (2018). Sustainable boron nitride nanosheet-reinforced cellulose nanofiber
454 composite film with oxygen barrier without the cost of color and cytotoxicity.
455 *Polymers*, 10(5), 501.

456 Niinivaara, E., & Cranston, E. D. (2020). Bottom-up assembly of nanocellulose
457 structures. *Carbohydrate Polymers*, 247, 116664.

458 Nomura, S., Kugo, Y., & Erata, T. (2020). ¹³C NMR and XRD studies on the

459 enhancement of cellulose II crystallinity with low concentration NaOH post-
460 treatments. *Cellulose*, 27(7), 3553-3563.

461 O'Sullivan, A. C. (1997). Cellulose: the structure slowly unravels. *Cellulose*, 4(3), 173-
462 207.

463 Park, S. A., Jeon, H., Kim, H., Shin, S. H., Choy, S., Hwang, D. S., . . . Oh, D. X.
464 (2019). Sustainable and recyclable super engineering thermoplastic from
465 biorenewable monomer. *Nature Communications*, 10(1), 2601.

466 Patil, S., Mahapatra, A., Gotmare, V. D., Patil, P. G., Bharimalla, A. K., & Arputharaj,
467 A. (2019). Effect of different mercerization techniques on tactile comfort of
468 cotton fabric. *Indian Journal of Fibre & Textile Research*, 44(2), 217-222.

469 Peng, L., Xu, Z., Liu, Z., Guo, Y., Li, P., & Gao, C. (2017). Ultrahigh thermal
470 conductive yet superflexible graphene films. *Advanced Materials*, 29(27),
471 1700589.

472 Sharma, S., Nair, S. S., Zhang, Z., Ragauskas, A. J., & Deng, Y. L. (2015).
473 Characterization of micro fibrillation process of cellulose and mercerized
474 cellulose pulp. *RSC Advances*, 5(77), 63111-63122.

475 Shen, H., Guo, J., Wang, H., Zhao, N., & Xu, J. (2015). Bioinspired modification of h-
476 BN for high thermal conductive composite films with aligned structure. *ACS*
477 *Applied Materials & Interfaces*, 7(10), 5701-5708.

478 Shim, J., Kim, H. J., Kim, B. G., Kim, Y. S., Kim, D. G., & Lee, J. C. (2017). 2D boron
479 nitride nanoflakes as a multifunctional additive in gel polymer electrolytes for
480 safe, long cycle life and high rate lithium metal batteries. *Energy &*
481 *Environmental Science*, 10(9), 1911-1916.

482 Tsai, M. H., Tseng, I. H., Chiang, J. C., & Li, J. J. (2014). Flexible polyimide films
483 hybrid with functionalized boron nitride and graphene oxide simultaneously to
484 improve thermal conduction and dimensional stability. *ACS Applied Materials*
485 *& Interfaces*, 6(11), 8639-8645.

486 Uetani, K., Okada, T., & Oyama, H. T. (2015). Crystallite size effect on thermal

487 conductive properties of nonwoven nanocellulose sheets. *Biomacromolecules*,
488 16(7), 2220-2227.

489 Wang, H. Y., Li, D. G., Yano, H., & Abe, K. (2014). Preparation of tough cellulose II
490 nanofibers with high thermal stability from wood. *Cellulose*, 21(3), 1505-1515.

491 Wang, M. J., Jiao, Z. Y., Chen, Y. P., Hou, X., Fu, L., Wu, Y. M., . . . Yu, J. H. (2018).
492 Enhanced thermal conductivity of poly(vinylidene fluoride)/boron nitride
493 nanosheet composites at low filler content. *Composites Part A: Applied Science
494 and Manufacturing*, 109, 321-329.

495 Wang, X., Bian, H., Ni, S., Sun, S., Jiao, L., & Dai, H. (2020). BNNS/PVA bilayer
496 composite film with multiple-improved properties by the synergistic actions of
497 cellulose nanofibrils and lignin nanoparticles. *International Journal of
498 Biological Macromolecules*, 157, 259-266.

499 Wang, X., Sun, M., Wang, R., Jiao, L., Bian, H., & Dai, H. (2022). Promoting h-BN
500 dispersion in cellulose-based composite by lignosulfonate for regulatable
501 effectual thermal management. *Materials & Design*, 214, 110379.

502 Wang, X., Yu, Z., Bian, H., Wu, W., Xiao, H., & Dai, H. (2019). Thermally conductive
503 and electrical insulation BNNS/CNF aerogel nano-paper. *Polymers*, 11(4), 660.

504 Wang, Z. D., Priego, P., Meziani, M. J., Wirth, K., Bhattacharya, S., Rao, A., . . . Sun,
505 Y. P. (2020). Dispersion of high-quality boron nitride nanosheets in
506 polyethylene for nanocomposites of superior thermal transport properties.
507 *Nanoscale Advances*, 2(6), 2507-2513.

508 Wang, Z. G., Wei, X., Bai, M. H., Lei, J., Xu, L., Huang, H. D., . . . Li, Z. M. (2021).
509 Green production of covalently functionalized boron nitride nanosheets via
510 saccharide-assisted mechanochemical exfoliation. *ACS Sustainable Chemistry
511 & Engineering*, 9(33), 11155-11162.

512 Wu, K., Fang, J., Ma, J., Huang, R., Chai, S., Chen, F., & Fu, Q. (2017). Achieving a
513 collapsible, strong, and highly thermally conductive film based on oriented
514 functionalized boron nitride nanosheets and cellulose nanofiber. *ACS Applied*

515 *Materials & Interfaces*, 9(35), 30035-30045.

516 Wu, K., Liao, P., Du, R. N., Zhang, Q., Chen, F., & Fu, Q. (2018). Preparation of a
517 thermally conductive biodegradable cellulose nanofiber/hydroxylated boron
518 nitride nanosheet film: the critical role of edge-hydroxylation. *Journal of*
519 *Materials Chemistry A*, 6(25), 11863-11873.

520 Xiao, F., Naficy, S., Casillas, G., Khan, M. H., Katkus, T., Jiang, L., . . . Huang, Z.
521 (2015). Hydrogels: Edge-hydroxylated boron nitride nanosheets as an effective
522 additive to improve the thermal response of hydrogels (*Adv. Mater.* 44/2015).
523 *Advanced Materials*, 27(44), 7247-7247.

524 Xu, Y., Yang, S., Zhao, P., Wu, M., Song, X., & Ragauskas, A. J. (2021). Effect of
525 endoglucanase and high-pressure homogenization post-treatments on
526 mechanically grinded cellulose nanofibrils and their film performance.
527 *Carbohydrate Polymers*, 253, 117253.

528 Yan, Q., Dai, W., Gao, J., Tan, X., Lv, L., Ying, J., . . . Lin, C.-T. (2021). Ultrahigh-
529 aspect-ratio boron nitride nanosheets leading to superhigh in-plane thermal
530 conductivity of foldable heat spreader. *ACS Nano*, 15(4), 6489-6498.

531 Yu, C. P., Zhang, Q. C., Zhang, J., Geng, R. J., Tian, W., Fan, X. D., & Yao, Y. G.
532 (2018). One-step in situ ball milling synthesis of polymer-functionalized few-
533 layered boron nitride and its application in high thermally conductive cellulose
534 composites. *ACS Applied Nano Materials*, 1(9), 4875-4883.

535 Zhang, K., Tao, P., Zhang, Y., Liao, X., & Nie, S. (2019). Highly thermal conductivity
536 of CNF/AlN hybrid films for thermal management of flexible energy storage
537 devices. *Carbohydrate Polymers*, 213, 228-235.

538 Zhao, D., Huang, J., Zhong, Y., Li, K., Zhang, L., & Cai, J. (2016). High-strength and
539 high-toughness double-cross-linked cellulose hydrogels: A new strategy using
540 sequential chemical and physical cross-linking. *Advanced Functional Materials*,
541 26(34), 6279-6287.

542